Computational Simulation of Airfoils Stall Aerodynamics at Low Reynolds Numbers

M.Sereez*, N.B. Abramov† and M.G.Goman‡

Faculty of Technology, De Montfort University, Leicester, UK

A.N.Khrabrov§

Central Aerohydrodynamic Institute (TsAGI), Zhukovsky, Russia

Experimental results for aerodynamic static hysteresis at stall conditions obtained in the TsAGI's T-124 low-turbulence wind tunnel for NACA0018 are presented and analysed. Computational predictions of aerodynamic static hysteresis are made using the OpenFOAM simulations considering different grids, turbulence models and solvers. Comparisons of computational simulation results with experimental wind tunnel data are made for 2D NACA0018 and NACA0012 airfoils at low Reynolds numbers $Re = (0.3 - 1.0) * 10^6$**. The properties of the proposed phenomenological bifurcation model for simulation of aerodynamic loads at the existence of static hysteresis are discussed.**

I. Introduction

Accurate experimental and computational predictions of aerodynamic loads at stall conditions are now important in many aeronautical applications from design of wind turbines and micro air vehicles operating at low Reynolds numbers[1–3] to adequate simulation of stall and post-stall dynamics of modern transport aircraft at high Reynolds numbers for addressing the loss of control in flight (LOC-I) problem.[4]

Conventional wind tunnel tests and modern computational fluid dynamics (CFD) simulation methods are providing consistent and accurate predictions of aerodynamic loads at low angles of attack under attached flow conditions. They are much less reliable and regular

*PhD Student, School of Engineering and Sustainable Development
†Senior Research Fellow, School of Engineering and Sustainable Development
‡Professor, School of Engineering and Sustainable Development; AIAA Senior Member
§Head of Unsteady Aerodynamic Division, Flight Dynamics and Control Department

at high angles of attack with stall manifesting various separated flow structures. In different low speed wind tunnels results for the same geometry and Reynolds number can differ significantly. Many experimental studies show existence of the aerodynamic static hysteresis in variations of aerodynamic loads during pitch-up and pitch-down change of angle of attack.[1–3] Similar hysteretic loops are observed at variation of sideslip angle and this is associated with onset of asymmetric structures of separated flow.

The current paper presents analysis of experimental data from the TsAGI's low-turbulence T-124 wind tunnel obtained for 2D NACA0018 airfoil in static tests and during slow sweep variation of angle of attack at two Reynolds numbers $Re = 0.3 * 10^6$ and $Re = 0.7 * 10^6$. The main focus is made on existence of static hysteresis in the dependencies of aerodynamic coefficients C_L, C_D, C_m. The computational simulation of aerodynamic loads and prediction of static hysteresis is made using the OpenFOAM open source CFD software[10] with objective to find an appropriate computational framework for better prediction of aerodynamic loads at the presence of separated flow conditions. Special emphasis in this paper is made on computational prediction of static hysteresis phenomenon. The authors know only one publication,[6] which presented CFD prediction of static hysteresis for NACA0012 airfoil.

The phenomenological bifurcation model as an extension of models presented in[3,11] is proposed for simulation of aerodynamic loads at the existence of static hysteresis and its main properties are discussed.

II. Experimental observation of aerodynamic hysteresis

Experimental investigation of the aerodynamic hysteresis at stall conditions for the NACA0018 airfoil was carried out in the low-turbulence TsAGI T-124 wind tunnel. The wing model had a chord of $0.24m$ and a span of $1m$, which is equal to the width of wind tunnel closed working section (Fig.1, left). The level of turbulence of wind tunnel air flow was less than 0.05% at air speed $V = 40m/s$. Dynamic rig OVP-124 allows measuring the lift and drag forces, X_a, Y_a, along the air flow and in orthogonal to flow direction, and also the pitching moment M_z (Fig.1, right). The test measurements can be conducted with fixed angle of attack α, continuous sweep movement $\alpha(t)$ and in forced oscillations $\alpha(t) = \alpha_0 + \alpha_s \sin(2\pi f t)$, which can be conducted with different amplitudes ($\alpha_s \leq 20^0$) and frequencies of oscillation ($f \leq 5Hz$) by changing the crank radius and DC motor speed. The straight wing is mounted in bearings on the left and right end of its installation and its rotation is forced with a lever arm of radius r. The reaction forces F, X_R, Y_R, X_L, Y_L are measured from three strain guages slip rings inside two bearings and the lever arm. These measurements allow calculation of the lift and drag forces and also pitching moment:

$$\begin{aligned} X_a &= X_R + X_L + F\sin(\alpha) \\ Y_a &= Y_R + Y_L - F\cos(\alpha) \\ M_z &= Fr \end{aligned} \tag{1}$$

and the lift, drag and pitching moment coefficients $C_L(\alpha), C_D(\alpha), C_m(\alpha)$.

The wind tunnel tests results for $V = 40$m/s ($Re = 0.7 * 10^6$) are presented in Figs.2 and 3. On the left plot of Fig.2 the lift coefficient dependence on angle of attack from static tests (red circles between $\alpha = -5^0$ and $\alpha = 37^0$) and measured in continuous slow sweep motion (green lines between $\alpha = 0$ and $\alpha = 30^0$) clearly show the existence of static hysteresis with

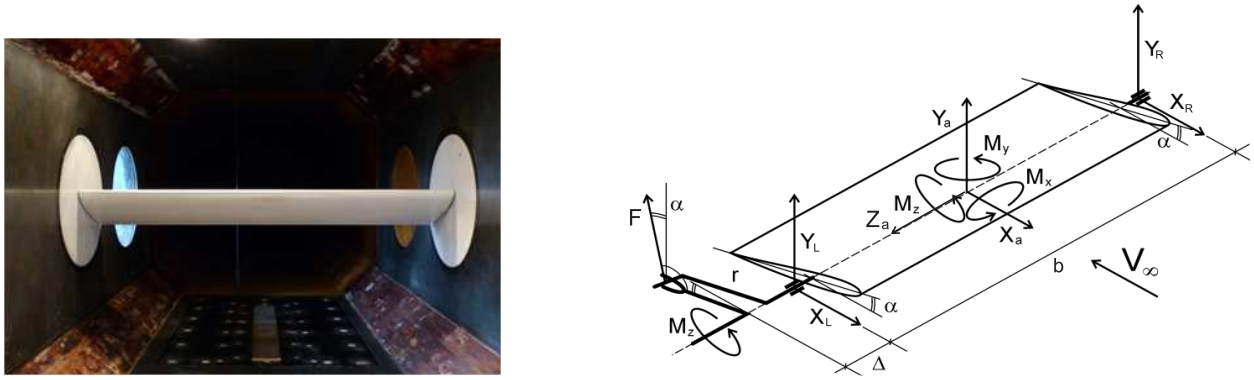

Figure 1: Straight wing with NACA-0018 airfoil fitted in the low-turbulence TsAGI T-124 wind tunnel (left plot). Force balancing scheme for measuring aerodynamic loads (right plot).

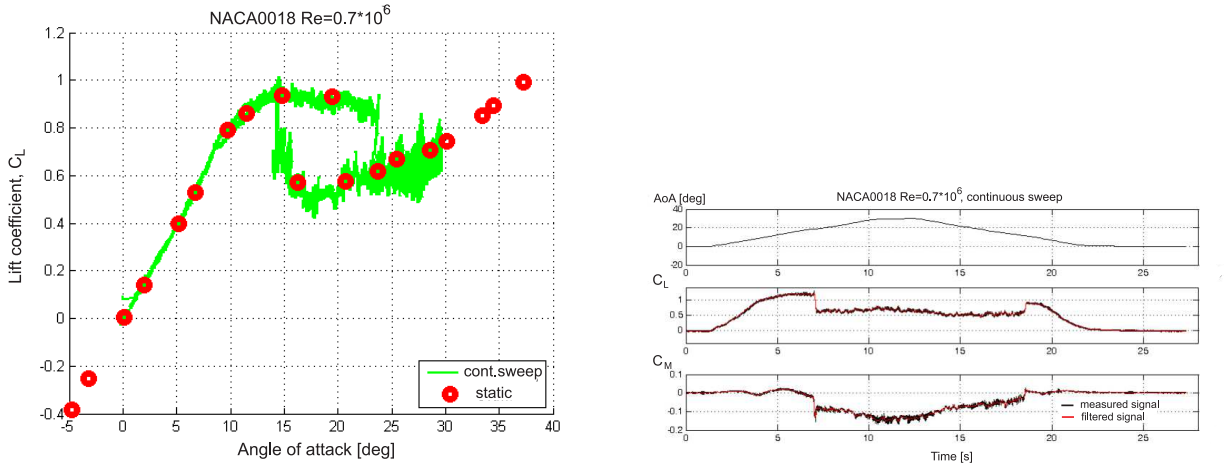

Figure 2: Dependence of the NACA0018 wing lift coefficient on angle of attack from static tests and continuous sweep motion (left), the angle of attack, lift and pitching moment coefficients time dependencies in continuous sweep motion (right). $V = 40m/s, Re = 700,000$.

two different branches for pitch-up and pitch-down angle of attack variation. The measured lift and pitching moment from continuous sweep variation of angle of attack are shown on the right plot of Fig.2 as functions of time. The static test points are calculated as averaged values of the measured aerodynamic load over some finite time interval, while the measured loads from continuous sweep motion are plotted directly without averaging and filtering.

The flow separation starts approximately at $\alpha = 10^0$, which is indicated by decline from the initial linear increase of the lift coefficient. High frequency variations in the measured lift and pitching moment (moderate amplitude at the higher branch of static hysteresis and increased amplitude at the lower branch of static hysteresis) are most likely connected with shedding of vortices having a positive or negative feedback effect on aerodynamic loading. The time dependencies on the right plot of Fig.2 show that the transitions between two branches of static hysteresis have abrupt and practically instantaneous nature probably reflecting the changes in structure of separated flow.

Fig. 3 shows the aerodynamic responses for the lift coefficient measured in forced oscil-

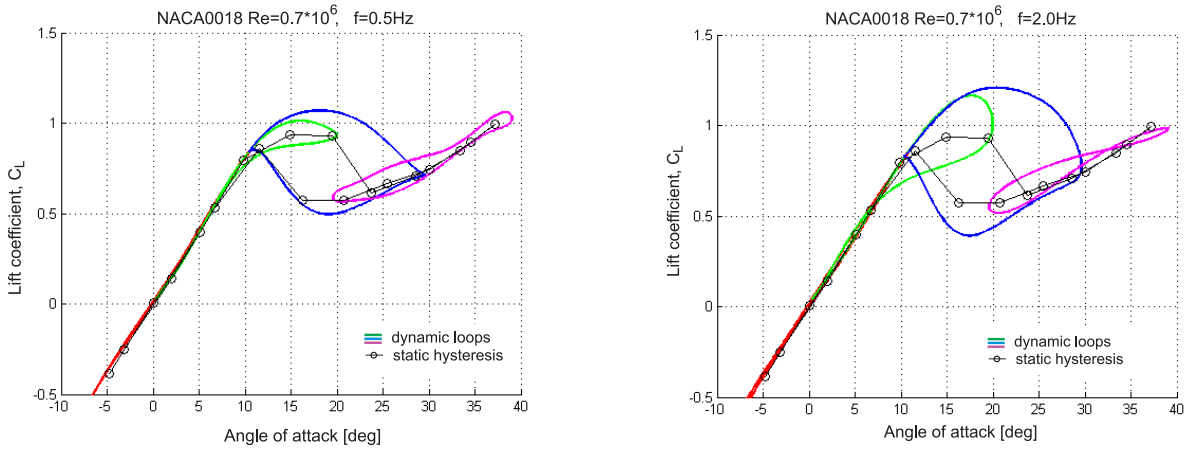

Figure 3: Dynamic loops in the NACA0018 wing lift coefficient during periodic changes of angle of attack with different amplitudes and frequencies: $f = 0.5Hz$ on the left, $f = 2.0Hz$ on the right. $V = 40m/s, Re = 700,000$.

lation tests with mean values of angle of attack $\alpha_0 = 10^0, 20^0, 30^0$ and amplitude $\alpha_s = 10^0$, which were averaged over a number of periods, smoothed and plotted on the graph against angle of attack for two different frequencies - $f = 0.5Hz$ (left plot) and $f = 2.0Hz$ (right plot). The dynamic loops marked by green and magenta lines belong to the top and the bottom branches of static hysteresis, respectively. The dynamic loops marked by blue lines are surrounding the observed static hysteresis and therefore transiting through regions with two different separating flow structures. The increase of frequency of oscillation expands dynamic loop on the top branch of static hysteresis (green lines) and dynamic loop surrounding static hysteresis loop (blue lines), but their growth is bounded by two boundaries, which correspond to the existence of different flow structure. One can reason that the upper part of dynamic loop is saturated by dependence of the lift coefficient corresponding to attached flow conditions and the bottom part of dynamic loop is saturated by the lift coefficient dependence corresponding to fully separated flow conditions. As a result the dynamic loops surrounding static hysteresis increase variation in the lift coefficient and include segments with extended to higher attitudes attached flow and to lower attitudes fully separated flow conditions. These two segments are separated by two segments with transitional flow structures. To better understand the flow transformations in static conditions and during airfoil's forced oscillations in stall region flow simulations using computational fluid dynamics methods are discussed in the following section.

III. CFD simulation of NACA0018 airfoil stall aerodynamics

The aerodynamics modeling and simulation based on the unsteady Reynolds-Averaged Navier-Stokes (URANS) equations are implemented in this paper using OpenFOAM, which is an open source CFD package written in C++ incorporating different numerical models, algorithms and CFD tools.[10] The URANS equations are normally closed using the semi-empirical turbulence models derived on the basis of various physical assumptions. The choice of the turbulence model influences the laminar-turbulent transition characteristics, onset of

flow separation, vortex shedding, etc. and therefore can affect the simulation of static hysteresis. Some turbulence models were available in OpenFOAM and some were added during the current study. The idea of using the open source software seems favorable due to its cost effectiveness and possibility for purposeful development with valuable feedback from an open community of users. OpenFOAM provides an efficient programming framework for computational fluid dynamics and computational tools development. Many turbulence models come along with OpenFOAM, for example commonly used models of Spalart-Allmaras (SA)[7] and the shear stress transport SST k-ω.[8] SST-V k-ω model .... has been programmed and incorporated during this study.

A. Computational Procedure

Accurate prediction of 2D airfoils' aerodynamics at stall conditions even at low Reynolds numbers is still a challenging problem. The right choice of governing equations, grid, turbulence model, solver and order of accuracy is important to obtain qualitatively correct and quantitatively acceptable results.

1. Mesh and boundary conditions

For 2D investigation of NACA0018/0012 airfoils the grid in the current study consisted of $140,402$ hexahedral elements with an initial 8 layers of constant cell height that represented $Y+ = 0.8$ with a cell normal height of $Y = 2e-05$m. The cell growth ratio from and to the airfoil was 1.05 and this enabled the proper capture of the boundary layer and a smooth transition of cells in the boundary layer to infinity. Far field was placed 40 times the chord length away in upstream, downstream, above and below the airfoil. $C-$ blocking was formulated with edges collapsed near the sharp trailing edge. Extreme care was taken in maintaining orthogonality, low aspect ratios and skewness which would ensure fast and accurate convergence in the solver.

2. Solvers

OpenFOAM implements Finite Volume Method (FVM) creating separated matrix equations which are solved using iterative solvers. The solution variables for each matrix equation are defined at centres of arbitrary shaped cells on unstructured grids. The Pressure-Implicit Split-Operator algorithm (PISO) is aimed for transient simulations solving the coupling problem for pressure and velocity equation and the Semi-Implicit Method for Pressure-Linked Equations (SIMPLE) algorithm is used for steady simulations. Steady state simulations were carried out using the simpleFoam solver on a basis of SIMPLE algorithm and the least squares formulation used to measure the gradients. Special schemes were used where applicable to keep the bounded quantities such as kinetic energy and specific dissipation within physical bounds.

3. Selection of turbulence model

The most commonly used turbulence models in external flows are one equation model Spalart-Allmaras[7] and the shear stress transport SST k-ω[9] were included in OpenFOAM.[10] The modified turbulence model SST-V k-ω[8] and transitional 3-Equation turbulence model

KKL-ω[9] were included in OpenFOAM in this study. The choice of the turbulence model, i.e. SA, SST/SST-V k-ω or KKL-ω and also the structure of computational mesh may strongly affect simulation of the aerodynamic static hysteresis and it is important to define the operational limits of the existing turbulence models and mesh generation to formulate recommendations for their practical use.

B. Prediction of aerodynamic static hysteresis

Aerodynamic static hysteresis observed experimentally in many wind tunnel investigations[1–3,6,12] is basically associated with transitions between two different structures of separated flow conditions, which can coexist at some range of angles of attack. The flow separation from an airfoil trailing edge starts above a laminar separation bubble region and develops a large separation region moving toward the airfoil leading edge. At some critical angle of attack this separated flow structure abruptly transforms to a massive separated flow covering the space between the leading and trailing edges shedding downstream large scale vortices and generating intensive buffeting. This massive separated flow structure continues at higher angles of attack and also remains in reverse pitch-down motion even after passing the angle of attack of abrupt fall from the upper branch.

1. Prediction of laminar separation bubble

A nonlinear behaviour of the lift and moment coefficients may occur at lower angles of attack due to laminar separation bubbles specific for low Reynolds numbers.[1] Figs.4 and 6 show experimentally tested dependencies for the lift coefficient $C_L(\alpha)$ at Reynolds numbers $Re = 0.3 * 10^6$ and $Re = 0.7 * 10^6$, respectively. The increase in slope C_{L_α} starts at $\alpha \approx 5^0$ and at $\alpha \approx 7^0$ the lift coefficient exceeds the linear development of C_L approximately on 25%. The increase in the lift coefficient and associated drag penalties are resulted from the development of a laminar separation bubble on the top surface of the airfoil, moving towards the leading edge as α increases. The separation bubble effect disappears roughly after $\alpha = 10^0$ followed by decrease in the lift coefficient slope. Further increase of angle of attack generates flow separation moving forward from the trailing edge.

In low angles of attack region $\alpha \leq 15^0$ steady state simulations using SIMPLE algorithm in combination with SST/SST-V k-ω turbulence models failed to predict the laminar separation bubble, they showed a linear increase in C_L against α until $\alpha = 10^0$. Opposite, the use of the transitional 3-Equation turbulence model, kkl-ω has allowed to predict the separation bubble effect. Steady state simulations using SIMPLE algorithm were carried out until $C_{L_{max}}$ at $\alpha = 15^0$.

2. NACA0018 airfoil stall at $Re = 0.3 * 10^6$.

In stall region unsteady simulations were carried out using transient SIMPLE foam (SIMPLE-transient) and PisoFoam (PISO) algorithm starting from $\alpha = 16$ degrees.[10] When transient SIMPLE Foam was used the maximum of CFL parameter (the CourantFriedrichsLewy stability criterion) was in between $5 - 50$ with at least $10 - 50$ linear iterations within a time step to reach a satisfactory convergence of flow parameters to some steady-state conditions. Once satisfactory convergence was achieved the solver proceeded to the next time step. When PISO algorithm was used nCorrectors was equal to 2 and Max CFL ≤ 1. Note that, PISO

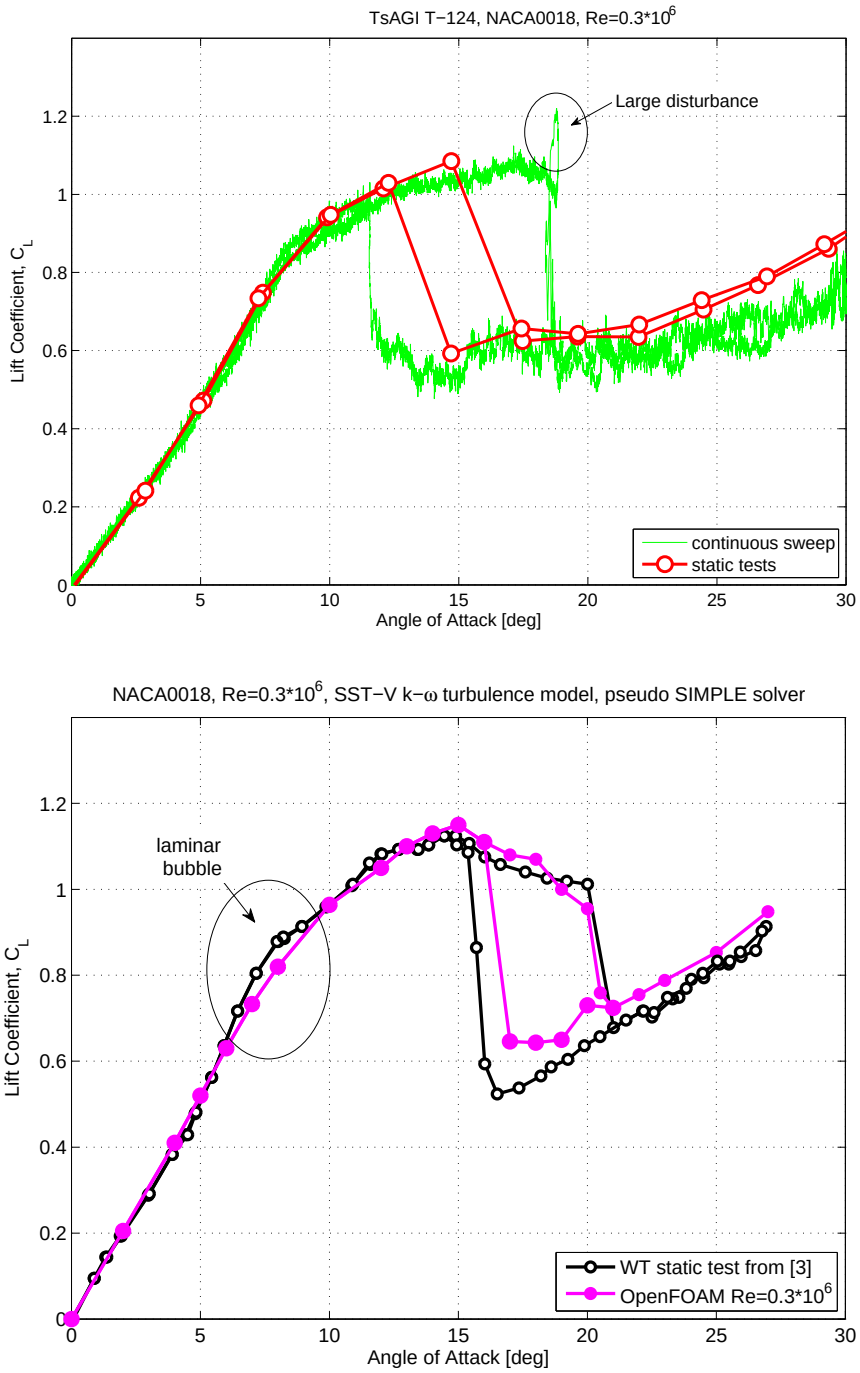

Figure 4: Experimental data for NACA0018 wing lift coefficient from TsAGI T-124 wind tunnel (top plot), experimental data from[3] vs OpenFoam prediction (bottom plot) at $Re = 0.3 * 10^6$.

algorithm is a non-iterative time advancement scheme which is why the Courant number of < 1 is a must and hence it is computationally very expensive to use. However, PISO algorithm is very robust and accurate for unsteady simulations.

The computational predictions of the static hysteresis phenomenon were compared with

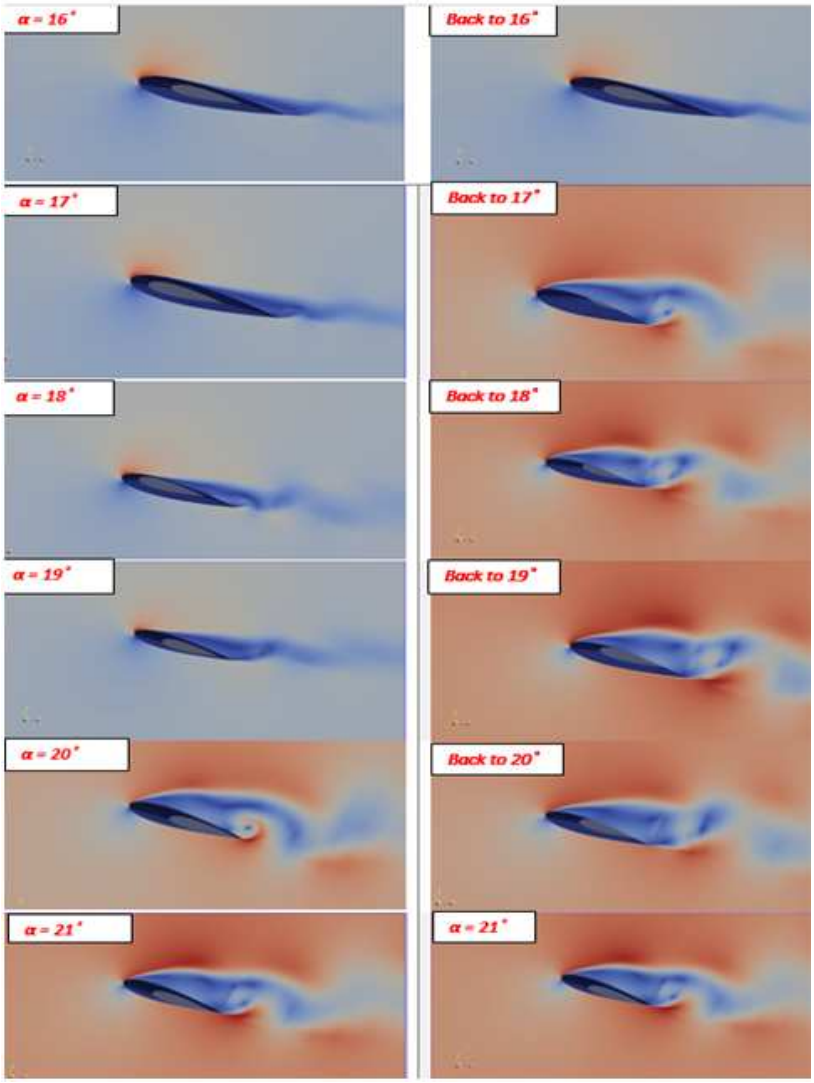

Figure 5: OpenFOAM flow patterns during angle of attack change in pitch-up (left column) and pitch-down (right column) for NACA0018 wing at $Re = 0.3 * 10^6$.

experimental data obtained in TsAGI's low turbulence wind tunnel T-124 and those published in[3] for a NACA0018 airfoil wing at $Re = 0.3 * 10^0$. The top plot in Fig.4 shows wind tunnel results from TsAGI's T-124 wind tunnel static tests (red circles) and continuous sweep variation of angle of attack (green line) for pitch-up and pitch-down motions. In static tests the change of angle of attack was implemented in two directions with increase of angle of attack (pitch-up motion) reaching maximum angle of attack $\alpha = 30^0 - 40^0$ and the following decrease of angle of attack (pitch-down motion) to return to the low angles of attack region. The measured aerodynamic loads in static tests at every fixed value of angle of attack are averaged over some time interval. A similar test conducted with very slow variation of angle of attack in pitch-up and pitch-down motions ($\dot{\alpha} = \pm 0.5$ deg/s) provides direct measurements of angle of attack and aerodynamic loads as functions of time. The measurements from continuous sweep motion (green line) indicate significant level of oscillations or buffeting above $\alpha = 10^0$ and especially after abrupt transition to a lower branch

of static hysteresis with much higher buffeting amplitude.

In continuous sweep motion the experimental data (green line) show a rather broad hysteresis loop ($\alpha = 12^0 - 18.5^0$) with transition from the top branch of static hysteresis to the bottom one at $\alpha = 18.5^0$ after action of large disturbance possibly due to shedding of large scale vortex. The return back to the upper branch happens at $\alpha = 12^0$. In static tests only one test point at $\alpha = 15^0$ indicated bistable states on two branches of static hysteresis. The experimental data from[3] presented in the bottom plot of Fig.4 also show a static hysteresis loop, but in the range of $\alpha = 16^0 - 20^0$, which is slightly more narrow than in the continuous sweep tests from TsAGI's T-124 wind tunnel.

The best simulation prediction of the static hysteresis phenomenon was carried out using SIMPLE solver with SST-V k-ω turbulence model, the result of this prediction is shown together with experimental data from[3] in the bottom plot of Fig.4.

The OpenFOAM simulation of the static hysteresis loop with SST-V k-ω turbulence model was rather successful for prediction of the upper branch of static hysteresis where flow separation develops from the trailing edge. The prediction of the lower branch with fully separated flow conditions and very high level of buffeting was not ideally matching the experimental data. For example, at $\alpha = 25^0$ the prediction is higher than the continuous sweep data on $\triangle C_L \approx 0.2$ and TsAGI's static on $\triangle C_L \approx 0.1$. The data from[3] for the lowest branch of static hysteresis is closer to the simulation prediction.

The major differences in simulation of static hysteresis are seen in prediction of angle of attack points where transitions between two branches of static hysteresis happen. The difficulties in accurate prediction of these critical points both in experimental tests and in CFD simulations are probably connected with the bifurcational nature of static hysteresis and its high sensitivity to physical or computational types of disturbances in proximity to bifurcation points.

The flow patterns predicted in the OpenFOAM simulations are shown in Fig. 5 for pitch-up (the left column) and pitch-down (the right column) variation of angle of attack. One can see that they are quite informative in explaining the existence of static hysteresis loops in the wing aerodynamic loads, in particular in $C_L(\alpha)$ dependence.

3. NACA0018 airfoil stall at $Re = 0.7 * 10^6$.

It is logical to expect that the increase of Reynolds number may affect airfoil stall characteristics and also complicate computational prediction especially for such a phenomenon as static hysteresis. The top plot in Fig.6 shows results from static tests and continuous sweep motion obtained in TsAGI's low turbulence wind tunnel T-124 at $Re = 0.7 * 10^6$. The results clearly demonstrate existence of static hysteresis, which is similar to the case for $Re = 0.3 * 10^0$ shown in Fig.4.

The increase of Reynolds number significantly widens the static hysteretic loop, for example, during continuous slow sweep variation of angle of attack in both directions the static hysteresis loop spans from $\alpha = 15^0$ till $\alpha = 24^0$, which is roughly 50% increase with respect to the hysteresis case at $Re = 0.3 * 10^6$. The wind tunnel static tests data also indicate the enlargement of hysteresis loop, but its width from $\alpha = 16^0$ till $\alpha = 19.5^0$ is less than in the case with continuous sweep motion. To reproduce in static tests more precisely the static hysteresis loop is required more testing points with small increment in angle of attack especially in proximity of bifurcation points.

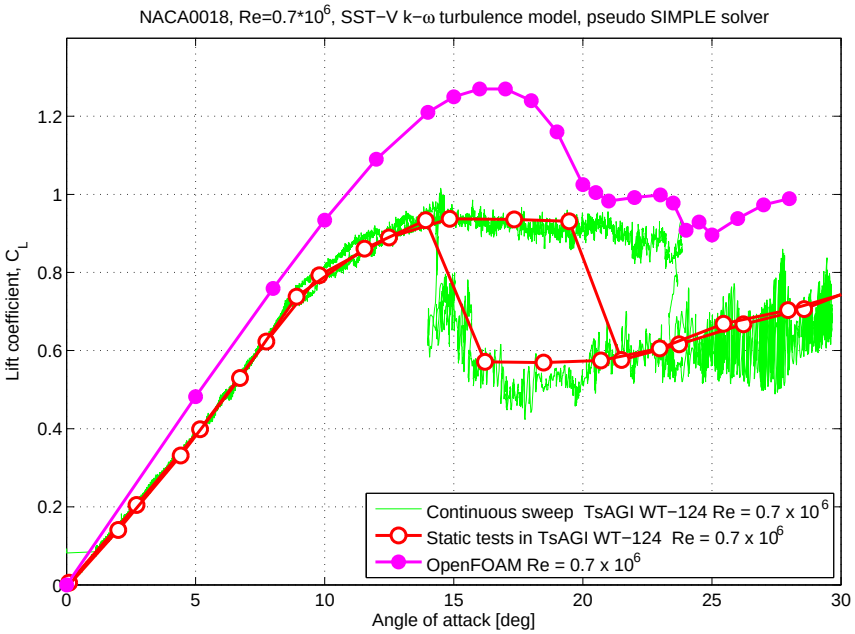

Figure 6: Experimental data for the NACA0018 wing lift coefficient from TsAGI T-124 wind tunnel vs OpenFOAM computational prediction results at $Re = 0.7 * 10^6$.

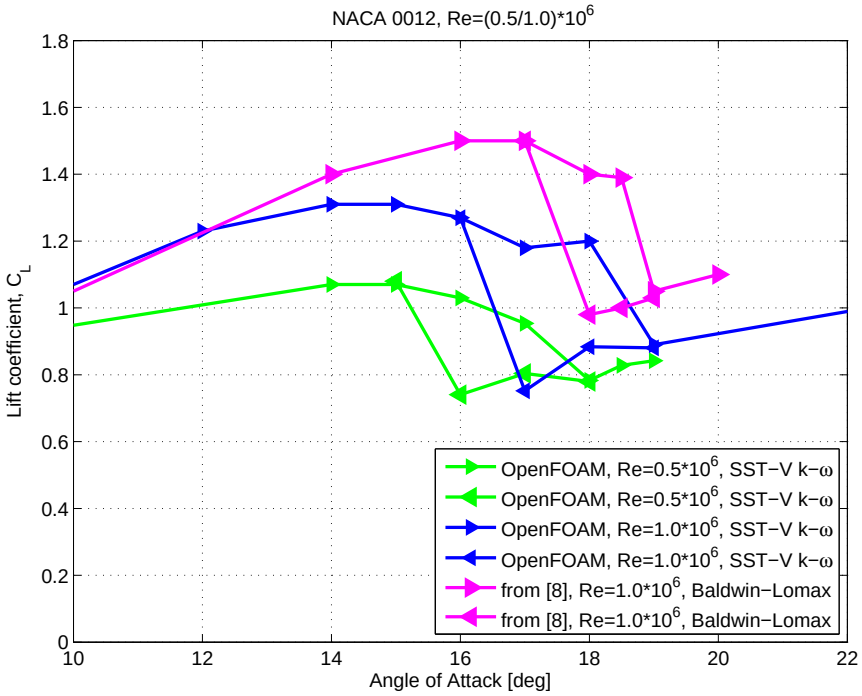

Figure 7: Computational simulation of the 2D NACA0012 airfoil lift coefficient with static hysteresis at $Re = (0.5/1.0) * 10^6$.

The OpenFOAM simulation of the NACA0018 wing stall characteristics at $Re = 0.7 * 10^6$ was carried out with SST-V k-ω turbulence model similar to the case with $Re = 0.3 * 10^6$. The predicted dependence for the lift coefficient $C_L(\alpha)$ during increase of angle of attack is substantially exceeding the maximum lift coefficient observed in experiment, the predicted maximum value $C_{L_{max}} = 1.26$ at $\alpha = 17^0$ is higher than in experiment on $\triangle C_L \approx 0.3$ (the top plot in Fig.6). After reaching the value $C_{L_{max}}$ there is a gradual drop in its value to the level of the upper branch of static hysteresis observed in experiment ($C_L \approx 1$), which is followed by another small drop exactly on the right side of static hysteresis loop. In reverse change of angle of attack from the plateau region with $\alpha = 22^0$ and from $\alpha = 28^0$ the implemented computational procedure failed to predict static hysteresis loop.

Comparing simulation and experimental results one can speculate that in the OpenFOAM simulation the flow separation was postponed to higher angles of attack with respect to experimental tests and this allowed to reach a higher magnitude of $C_{L_{max}}$. Also, in experiment the upper branch of static hysteresis corresponds to a separated flow structure, which is different from the fully developed separated structure on the bottom branch of static hysteresis and also different from the partially separated flow on the predicted by OpenFOAM dependence with $C_{L_{max}} = 1.26$. So, one can assume a possibility for existence of a triple-stable static hysteresis and for its visualization both in simulation and also in experimental testing it is required appropriate methodological adjustments.

4. NACA0012 airfoil stall at $Re = 0.5$ *and* $1.0 * 10^6$.

The bottom plot in Fig.7 shows the OpenFOAM simulation results with SST-V k-ω turbulence model for NACA0012 wing (blue lines for $Re = 1.0 * 10^6$ and green lines for $Re = 0.5 * 10^6$). For comparison on the same plot are given results of similar simulation with the algebraic Baldwin-Lomax turbulence model from[6] (magenta lines). The OpenFOAM simulations indicate the delay in angle of attack in stall development with increase of Reynolds number from $0.5 * 10^6$ to $1.0 * 10^6$. One can see the influence of the turbulence model used in simulation, at $Re = 1.0 * 10^6$ the Baldwin-Lomax turbulence model predicts flow separated at higher angle of attack than it was in OpenFoam prediction with SST-V k-ω turbulence model giving increase in the lift coefficient $\triangle C_L = 0.2$. However, in all three cases the static hysteresis loop in the lift dependence on angle of attack has been detected.

IV. Phenomenological bifurcation model of static hysteresis

Reduced order model for simulation of aerodynamic responses at the presence of static hysteresis can be developed with inclusion of its bifurcation properties. The state-space aerodynamic model for dynamic hysteresis accounting for flow transient processes proposed in[11]

$$\begin{aligned} C_L &= C_L(\alpha, x) \\ \tau_1 \frac{dx}{dt} + x &= x_0(\alpha - \tau_2 \dot{\alpha}) \end{aligned} \tag{2}$$

was modified in[3] by introduction of a two-valued function for position of flow separation point $x_{0_\pm}$ depending on angle of attack α and its rate of change $\dot{\alpha}$ in static conditions. This modification allows modeling aerodynamic responses at large amplitude oscillations covering hysteresis loop, but may fail to match behavior at critical states crossing and action of

external disturbances. To capture these properties in[13] was proposed a nonlinear differential equation for variable x inherently possessing bifurcation properties of static hysteresis, which include variation of characteristic time scale in proximity of bifurcation points and separation of regions of attraction for the upper and lower branches of static hysteresis. Here just a general idea of this approach is briefly outlined. The linear differential equation from (2) is replaced by the following nonlinear equation in the form of cubic polynomial with respect to relative deviation of variable x from its static position x_0:

$$\frac{dx}{dt} = G(x, \alpha, \dot{\alpha}) = k_1(\alpha)(x_0 - x) + k_2(\alpha)(x_0 - x)^2 + k_3(\alpha)(x_0 - x)^3 \tag{3}$$

where $k_1 = 1/\tau_1$ and x_0 depends on shifted argument $\alpha_s = \alpha - \tau_2\dot{\alpha}$.

The modified model (2),(3) intrinsically possesses the properties required for modelling aerodynamic responses with static hysteresis, i.e. following the static hysteresis branches at slow variation of angle of attack in pitch-up/pitch-down motions with abrupt jumps from one branch to another in bifurcation points, showing a higher time lag during critical states crossings, and separating domains of attraction for upper and lower branches of static hysteresis, the latter property is responsible for the model sensitivity to external disturbance in proximity of bifurcation points making the static hysteresis loop width dependent on the level of turbulence and the wing structural vibrations in wind tunnel tests.

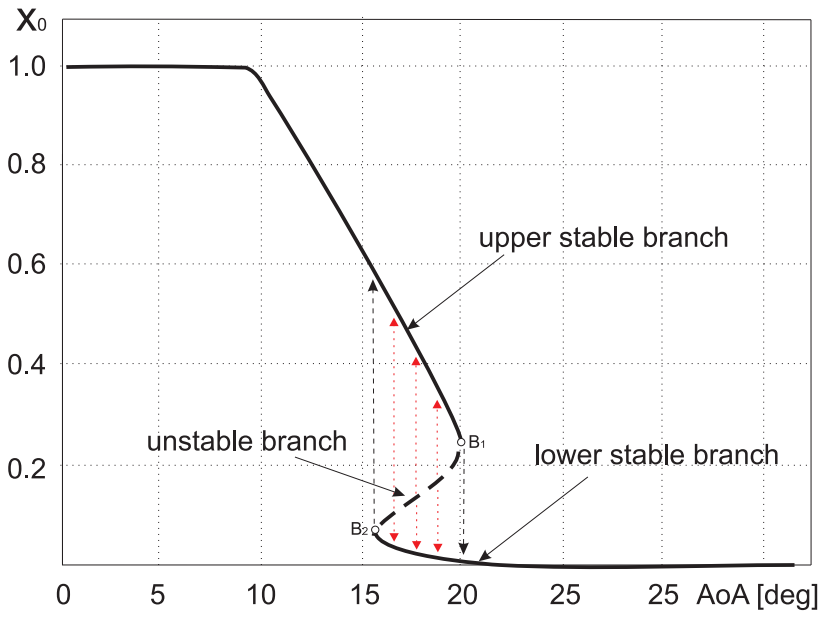

Figure 8: Bifurcation model of static hysteresis with two stable branches separated by unstable branch.

The identification of functions $k_i(\alpha), i = 1, 2, 3$ in (3) requires use of various experimental data, for example shape of stable hysteresis loop branches, unsteady aerodynamic derivatives from forced oscillation tests with small amplitudes measured on both branches of static hysteresis and also aerodynamic responses from forced oscillation tests with large amplitudes with critical states crossing covering static hysteresis loop.[13] Fig.8 shows two stable branches of static hysteresis smoothly connected by one unstable branch, which plays a role of a separatrix dividing regions of attraction for two stable branches of stable hysteresis (see red

transition arrows). The continuous curve of stable and unstable branches of static hysteresis shown in Fig.8 is defined by the following condition:

$$G(x, \alpha_s) = 0 \tag{4}$$

In nonlinear system (3) the effective local time scale on a stable branch is inversely proportional to the partial derivative $\tau_1 = 1/\left(\frac{\partial F}{\partial x}\right)\|_{G=0}$, calculated in a point belonging to the branch. In regular points on stable branches the characteristic time scale in the linearised model (2) is defined as $\tau_1(\alpha) = 1/k_1(\alpha)$, while in close proximity of bifurcation points B_1, B_2 the characteristic time scale is approaching infinity $\tau_1 \to \infty$, which slows down transitions from critical states B_1 and B_2 to the opposite branch. The proposed nonlinear transformation of model (2) has been successfully validated on experimental data with static hysteresis for NACA0018 wing with aspect ratio $A = 5$, which were presented in[12] and the modelling results can be found in.[13]

V. Conclusions

The presented experimental wind tunnel data for the NACA 0018 airfoil at $Re = (0.3 - 0.7) * 10^6$ show existence of the static hysteresis loop in the aerodynamic loads during pitch-up and pitch-down variations of angle of attack. The width of static hysteresis loop is different in static tests and during slow sweep variation of angle of attack indicating sensitivity of abrupt transitions between different separated flow structures to wind tunnel test conditions. The computational simulation using the OpenFOAM with SST-V k-ω turbulence model of the NACA 0018 airfoil stall aerodynamics revealed the existence of static hysteresis dependence for $Re = 0.3 * 10^6$ and failed to predict static hysteresis at $Re = 0.7 * 10^6$. The predicted static hysteresis loop matches well with the experimental results from[3] and shows a narrower loop in comparison with the TsAGI's wind tunnel results obtained in slow variation of angle of attack. The computational prediction of aerodynamic static hysteresis for the NACA 0012 airfoil was successful at $Re = (0.5 - 1.0) * 10^6$ and showed the advantage of using the simple algebraic Baldwin-Lomax turbulence model. The conducted experimental and computation studies of aerodynamic static hysteresis with transitions between various separated flow structures show the need in further investigations in this area. The proposed phenomenological bifurcation model for simulation of aerodynamic loads with static hysteresis may be tuned using experimental and computational data and used as a low cost reduced order model for stall flow conditions.

References

[1]Zifeng Yang, Hirofumi Igarashi, Mathew Martin and Hui Hu. *An Experimental Investigation on Aerodynamic Hysteresis of a Low-Reynolds Number Airfoil.* AIAA-2008-0315, 46th AIAA Aerospace Sciences Meeting and Exhibit, Jan 7-10, 2008, Reno, Nevada. J. Fluids Eng 130(5), 051101 (Apr 25, 2008) (11 pages), doi:10.1115/1.2907416

[2]W.A.Timmer. *Two-dimensional low-Reynolds number wind tunnel results for airfoil NACA 0018.* Wind Engineering Volume 32, No. 6, 2008, pp. 525-537.

[3]David R. Williams, Florian Reisner, David Greenblatt, Hanns Muller-Vahl, Christoph Strangfeld.

Modeling Lift Hysteresis with a Modified Goman-Khrabrov Model on Pitching Airfoils. AIAA-2015-2631, 45th AIAA Fluid Dynamics Conference, 22-26 June 2015, Dallas, TX.

[4]Simulation of Upset Recovery in Aviation. EU 7th Framework Program Research project 2009-2012. http://www.supra.aero/home.htm

[5]Dirk M.Luchtenburg, Clarence W.Rowley, Mark W.Lohry, Luigi Martinelli, and Robert Stengel. *Unsteady High-Angle-of-Attack Aerodynamic Model of a Generic Jet Transport*. Journal of Aircraft, Vol. 52, No. 3, May-June 2015.

[6]Sanjay Mittal, Priyank Saxena. *Hysteresis in flow past a NACA 0012 airfoil*. Comput. Methods Appl. Mech. Engrg. 191 (2002) 2179-2189.

[7]Spalart, P. R. and Allmaras, S. R., "A One-Equation Turbulence Model for Aerodynamic Flows," Recherche Aerospatiale, No. 1, 1994, pp. 5-21.

[8]Menter, F. R. (1993), "Zonal Two Equation k- Turbulence Models for Aerodynamic Flows", AIAA Paper 93-2906.

[9]Menter, F. R., "Improved Two-Equation k-omega Turbulence Models for Aerodynamic Flows," NASA TM 103975, October 1992

[10]OpenFOAM. The open source computational fuid dynamics toolbox, 2013. http://www.openfoam.com/.

[11]M Goman, A Khrabrov "State-space representation of aerodynamic characteristics of an aircraft at high angles of attack", Journal of Aircraft, Vol. 31, Issue 5, pp. 1109-1115.

[12]A.Khrabrov, K.Kolinko, O.Miatov, A.Zhuk *Experimental Investigation of Wings Unsteady Aerodynamics at Flow Separation regimes*, TsAGI Preprint N86, 1997.

[13]N.B.Abramov, M.G.Goman, A.N.Khrabrov, and K.A.Kolinko, Simple Wings Unsteady Aerodynamics at High Angles of Attack: Experimental and Modelling Results, AIAA-99-4013, 1999.